





Open Archive Toulouse Archive Ouverte (OATAO)

OATAO is an open access repository that collects the work of Toulouse researchers and makes it freely available over the web where possible

This is an author's version published in: <http://oatao.univ-toulouse.fr/27435>

Official URL: <https://doi.org/10.1016/j.ensm.2020.05.032>

To cite this version:

Bai, Xue  and Iadecola, Antonella and Tarascon, Jean-Marie and Rozier, Patrick  *Decoupling the effect of vacancies and electropositive cations on the anionic redox processes in Na based P2-type layered oxides.* (2020) *Energy Storage Materials*, 31. 146-155. ISSN 24058297

Any correspondence concerning this service should be sent to the repository administrator: tech-oatao@listes-diff.inp-toulouse.fr

Decoupling the effect of vacancies and electropositive cations on the anionic redox processes in Na based P2-type layered oxides

Xue Bai^{a,c}, Antonella Iadecola^c, Jean-Marie Tarascon^{b,c}, Patrick Rozier^{a,c,*}

^a CIRIMAT, Université de Toulouse, CNRS, Université Toulouse 3 - Paul Sabatier, 118 Route de Narbonne, 31062, Toulouse cedex 9, France

^b Chimie du Solide et de l'Energie Collège de France, 11 Place Marcelin, Berthelot, 75231, Paris, France

^c RS2E, Réseau Français sur le Stockage Electrochimique de l'Energie, FR CNRS 3459, 80039, Amiens Cedex, France

ARTICLE INFO

Keywords:

Anionic redox
Na-ion batteries
Layered structure
Oxygen activity

ABSTRACT

The activation of anionic redox couple is recognized as one of the best way to increase the energy density of positive electrode materials in both Li and Na-ion batteries. However, for such hope, to materialize a better understanding of the parameters governing the activation, reversibility and efficiency of the anionic redox in NaMO₂ layered compounds is still sorely needed. Herein, we report a new P2- Na_{0.63}[□_{0.036}Mg_{0.143}Mn_{0.821}]O₂ compound that combines vacancies and Mg doping as well-known sources for anionic redox activation and benchmark its electrochemical performances against P2- Na_{0.72}[Mg_{0.31}Mn_{0.69}]O₂. We found that vacancies and Mg doping trigger independently anionic redox processes that differ in terms of redox voltage and reversibility. The one associated to vacancies occurs at the lowest potential and is irreversible. Moreover, we evidenced by monitoring the structural evolution of the pristine phase during cycling the benefice of anionic processes in ensuring the stabilization of P2-type structure at high voltage over a wide range in Na content. These findings highlight the importance of the anionic redox process origin (e.g. vacancies vs. highly electropositive cations) in governing the material electrochemical properties, while providing a new way to efficiently stabilize, without capacity loss, the P2-type structure through the charge process in non A-rich compounds.

1. Introduction

The activation of the anionic redox couple in Li based layered oxide is one of the best solution to improve the specific energy of the positive electrode materials [1–4]. However, the practical application of such anionic redox is still limited either due to O₂ release or the cation migration associated with the oxygen redox activity [5]. In parallel, the Na ion batteries are now recognized as one of the possibilities to replace, in dedicated range of application where gravimetric penalty is not a real concern, the LIBs and solve the issues of distribution of resources, cost and safety. The search for high energy density NIBs is then ongoing and the development of layered NaMO₂ compounds exhibiting cumulative cationic and anionic redox couples is investigated. Since the first evidence of anionic redox in the model Na rich compound Na₂RuO₃ allowing to evidence that Na, as Li, can activate the anionic redox [6,7], the participation of non bonding |O_{2p} states to the capacity has also been reported in Na deficient Na_xMO₂, where the M sites are partially occupied by earth alkaline (Mg) [8], vacancies [9–11] or more

electronegative Zn ions [12]. Taking benefit, in the case of Na based layered oxides, of the wide possibility to tune chemical composition of the transition metal layer, we decided to investigate the effect of the combination of different species known to trigger oxygen oxidation on the behavior of anionic redox couple.

Anionic redox in AMO₂ layered oxides (A = Li, Na and M = transition metal) has been shown to arise from the occurrence of O(2p) non bonding orbitals created by substituting part of the transition metal by species engaging ionic bonds with O so that electrons on these bonds are mainly localized on the oxygen anions. Among possibilities to activate anionic redox, vacancies in the transition metal sites are known to lead to whether reversible or irreversible anionic redox process when their distribution is respectively ordered [9] or disorder [11]. The absence of positive charge in the vacant site can be considered as leading to the limit situation where electrons are fully localized on oxygen anions and so that the corresponding non bonding |O_{2p} states should present the highest energy. At the opposite, the +2 charge carried out by Mg or Zn species, both known to activate anionic redox, should bring the non bonding |O_{2p} states deeper in energy,

* Corresponding author. CIRIMAT, Université de Toulouse, CNRS, Université Toulouse 3 - Paul Sabatier, 118 Route de Narbonne, 31062, Toulouse cedex 9, France.
E-mail addresses: bai@chimie.ups-tlse.fr (X. Bai), antonella.iadecola@synchrotron-soleil.fr (A. Iadecola), jean-marie.tarascon@college-de-france.fr (J.-M. Tarascon), rozier@chimie.ups-tlse.fr (P. Rozier).

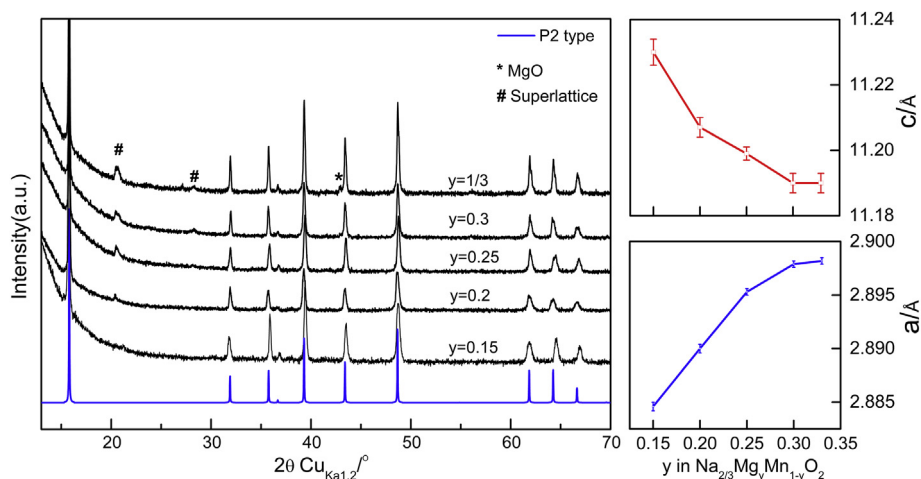


Fig. 1. (a) Evolution of XRD patterns of P2 type $\text{Na}_{2/3}[\text{Mg}_y\text{Mn}_{1-y}]\text{O}_2$ with $y = 0.15, 0.2, 0.25, 0.3, 1/3$ and calculated one using the structure data from P2 type structure. (b) Evolution of refined cell parameters a and c with the amount of Mg.

causing an energy difference with that of vacancies related one, large enough to be distinguishable. Mg and Zn doping being reported to lead to fully reversible anionic process and Mg showing, contrary to Zn, no cation migration along cycling, we decided to synthesize a mixed vacancy/Mg doped layered compound to study the effect of the combination of two sources for anionic redox activation on the overall electrochemical behavior. Most of anionic redox specificities such as efficiency, reversibility and structure changes being observable during the first activation of the process, the studies focus on the first charge/discharge behavior of model compounds P2 $\text{Na}_{2/3}[\text{Mn}_{1-y}\text{Mg}_y]\text{O}_2$ targeting Mn in not active +4 valence state to minimize cationic redox contribution.

Here we show the successful synthesis of mixed vacancy/Mg layered oxide P2 $\text{Na}_{0.63}[\square_{0.036}\text{Mg}_{0.143}\text{Mn}_{0.820}]\text{O}_2$ which exhibits two distinct oxygen redox activities both in terms of voltage and reversibility. The comparison of the electrochemical behavior with that of purely Mg doped P2 $\text{Na}_{0.72}[\text{Mg}_{0.31}\text{Mn}_{0.69}]\text{O}_2$ compound used as reference, allows attributing each process to the vacancy or Mg activated anionic redox couple and demonstrates that they act in an independent way. The investigation of structural changes during the first charge/discharge process allows confirming the benefit of anionic redox activation on the stabilization of the P2 structure at high state of charge with a clear postponement or even suppression of the P2 to O2 structure change. This stabilizing effect occurring while anionic redox is active allows maintaining capacity opposite to the loss observed when non active element such as Al^{3+} are used to prevent access to high state of charges.

2. Material and methods

2.1. Material synthesis and chemical quantification

The series of $\text{Na}_{2/3}\text{Mg}_y\text{Mn}_{1-y}\text{O}_2$ with $y = 0.15, 0.2, 0.25, 0.3, 0.33$ were prepared via solid state reaction between Na_2CO_3 (>99.5% Aldrich) with 5 wt% excess and stoichiometric amounts of $(\text{MgCO}_3)_4$ $\text{Mg}(\text{OH})_2 \cdot 5\text{H}_2\text{O}$ (99.99% Aldrich) and Mn_2O_4 (>97%). The reactants were ball milled altogether for 30min in SPEX miller at 1725 rpm with $r_{\text{ball/powder}}$ weight ratio of 7 and heat treated at 900 °C for 12h with the ramping rate of 5 °C/min. The cooling procedure adapted to allow creation of vacancies as already reported [1,2,9,13] follows first the furnace inertia down to 400 °C and the samples are then quenched and placed in a desiccator to avoid any side reaction with moisture before transferring to glove box for further handling. The chemical composition of the samples were determined using an Inductively Coupled Plasma/atomic emission spectrometry (ICP AES) spectrometer (Varian 720 ES Optical

Emission Spectrometer). Mn oxidation state was determined by iodometry using the Murray method [14,15].

2.2. Structural characterization

All X ray powder diffraction patterns were collected using a Bruker D8 diffractometer equipped with a $\text{Cu K}\alpha$ radiation source. The *operando* XRD was performed with a Swagelok type cell equipped with a Beryllium window protected by an aluminum foil as current collector. The cell is cycled at C/30 (1 Na exchange in 30 h) and each scan covers a range of 2θ from 10° to 50° in a duration of 1 h. Rietveld refinements are performed using FullProf software.

2.3. Electrochemical characterization

The electrochemical tests were carried out in Swagelok type cell. The pristine materials were ball milled with 20% super P carbon black for 30 min to ensure a homogeneous mixture and to prevent for large polarization. A sodium metal foil pressed onto stainless steel current collector was used as a negative electrode. The galvanostatic and voltammetric techniques were carried out using Biologic potentiostat/galvanostat. The cycling rates were calculated using the theoretical capacity to remove 1 Na as 1 C rate. The half cells were cycled at C/20, unless otherwise mentioned. Voltammetric techniques (cyclic voltammetry and linear voltammetry) were conducted in three electrodes Swagelok cell with both Na metal casted on the stainless steel plungers as reference and counter electrodes. All the electrochemical tests were duplicated at least twice to get reproducible results.

2.4. XAS measurements

Ex situ XAS measurements at the Mn K edge were performed in transmission mode at the ROCK beamline of synchrotron SOLEIL (France) [16]. A Si (111) channel cut quick XAS monochromator with an energy resolution of 0.65 eV at 6.5 keV and an oscillating frequency of 2 Hz was used. The intensity of the monochromatic X ray beam was measured by three consecutive ionization detectors. A Mn foil was placed between the second and the third ionization chamber as reference. *Ex situ* samples were prepared as self standing films which were pre cycled at C/30, recovered from Swagelok cell, rinsed with DMC, dried in vacuum chamber and finally sealed in Kapton tape in glove box. *Ex situ* XAS spectra were treated using the Athena for energy calibration and normalization.

Table 1
Summary of compositional analyses for $\text{Na}_x\text{Mg}_y\text{Mn}_{1-y}\text{O}_2$ with $y = 0.3$ and 0.15

Sample	Mn ^{N+}	Na/Mg/Mn ratio	Composition
y 0.15	+3.76(2)	0.65/0.15/0.85	$\text{Na}_{0.63}[\square_{0.036}\text{Mg}_{0.143}\text{Mn}_{0.82}]\text{O}_2$
y 0.3	+3.86(2)	0.72/0.311/0.689	$\text{Na}_{0.72}[\text{Mg}_{0.31}\text{Mn}_{0.69}]\text{O}_2$

3. Results

3.1. Structure and chemical composition analysis

The X ray diffraction (XRD) patterns of the $\text{Na}_{2/3}[\text{Mg}_y\text{Mn}_{1-y}]\text{O}_2$ samples with $y = 0.15, 0.2, 0.25, 0.3, 0.33$ reported in Fig. 1 and compared with calculated one using structure data reported by Delmas [17] show that all samples correspond to P2 type layered structure. The XRD pattern for sample with $y = 0.33$ shows extra peaks corresponding to MgO impurity which indicates that the limit of the solid solution domain is restricted to y

0.3 in agreement with reported data [8,18]. Extra asymmetric and broad diffraction peaks (marked as # in Fig. 1a) exhibiting increasing intensity with increasing Mg content indicate the partial and progressive ordering of Mg/Mn distribution [18]. However, for conciseness, the small hexagonal unit cell (Space Group $P6_3/mmc$, $a = 2.9 \text{ \AA}$, $c = 11.2 \text{ \AA}$) describing the average structure with random distribution of species in the transition metal layer is used to refine all structures. Lowest ($y = 0.15$) and highest ($y = 0.3$) Mg content are selected for deeper analysis. The atomic ratio of cation species is determined using ICP (Table S1) and the Mn valence state is determined by titration techniques. The combination of data summarized in Table 1 shows that for $y = 0.15$ sample, to balance the Mn valence state, the presence of vacancies has to be taken into account and leads to the compositions $\text{Na}_{0.63}[\square_{0.036}\text{Mg}_{0.143}\text{Mn}^{3+}_{0.196}\text{Mn}^{4+}_{0.624}]\text{O}_2$. For the sample

with high, $y = 0.3$, Mg content, the balance of Mn valence state agrees with the absence of Mn defects leading to the formula $\text{Na}_{0.72}[\text{Mg}_{0.31}\text{Mn}^{3+}_{0.097}\text{Mn}^{4+}_{0.593}]\text{O}_2$. Rietveld refinement using Fullprof software was performed using the structure data of the average structure (space group $P6_3/mmc$) as initial model. For the accuracy of the refinement, the occupancy of the two Na sites and of the sites shared by Mg/Mn are constrained in such a way that the sum is fixed to the stoichiometry given by ICP. Thermal displacement parameters of Na ions and of Mg/Mn are constrained to be identical. Once all parameters refined, a final test confirms the absence of large divergence of the site occupancy from the chemical composition. The comparison of calculated and experimental XRD patterns is presented in Fig. 2 and reliability factors and refined structural parameters are summarized in Table 2. The Mg/Mn ratio calculated from refined occupancies confirms the stoichiometry $\text{Na}_{0.72}[\text{Mg}_{0.31}\text{Mn}_{0.69}]\text{O}_2$ for $y = 0.30$ sample, while, for $y = 0.15$, the contribution of cation vacancies has to be added and results in the stoichiometry $\text{Na}_{0.63}[\square_{0.036}\text{Mg}_{0.143}\text{Mn}_{0.82}]\text{O}_2$. The presence of vacancies in Mn based layered oxides is not a total surprise and agrees well with previously reported studies showing that tuning chemical synthesis parameters allows governing to some extent the amount of Mn defects [13].

3.2. Electrochemical behavior

The galvanostatic cycling in half cell versus Na was performed at C/20 (theoretical (de)intercalation of 1 Na^+ per $\text{Na}_x[\text{Mg}_y\text{Mn}_{1-y}]\text{O}_2$ in 20 h) in the voltage range [1.5–4.5 V] vs. Na^+/Na^0 at room temperature. The voltage composition curves are presented in Fig. 3a and Fig. 3b for respectively $y = 0.3$ and $y = 0.15$ samples. They both show a first sloping domain associated to the extraction of 0.1 and 0.2 Na for respectively $y = 0.3$ and $y = 0.15$) which agrees well with oxidation of remaining Mn^{3+}

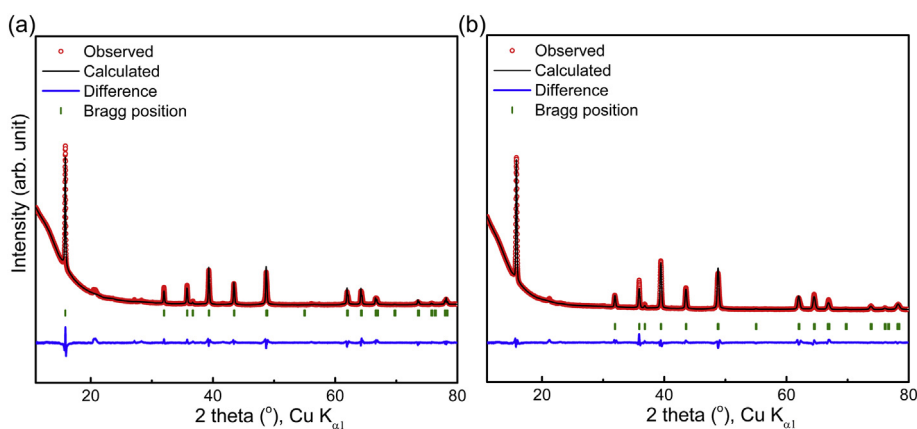


Fig. 2. Results of Rietveld refinement of XRD patterns of P2-type a) $\text{Na}_{0.72}[\text{Mg}_{0.31}\text{Mn}_{0.69}]\text{O}_2$ and b) $\text{Na}_{0.63}[\square_{0.036}\text{Mg}_{0.143}\text{Mn}_{0.82}]\text{O}_2$ based on S.G. $P6_3/mmc$.

Table 2

Refined crystallographic parameters for (a) P2- $\text{Na}_{0.72}[\text{Mg}_{0.31}\text{Mn}_{0.69}]\text{O}_2$ and (b) P2- $\text{Na}_{0.63}[\square_{0.036}\text{Mg}_{0.14}\text{Mn}_{0.82}]\text{O}_2$. The fixed parameters are marked with *.

(a) S.G.: $P6_3/mmc$		a	2.8966(1) \AA	c	11.191(1) \AA	Rwp	13.4	Rb	5.04	Rf	6.13	χ^2	7.08
Atom	Wyckoff positions	X	Y	Z	Biso(\AA^2)	Occup.							
Na_e	2d	1/3	2/3	3/4	3.6(2)	0.428(1)							
Na_f	2b	0	0	1/4	3.5(2)	0.292(1)							
Mn	2a	0	0	0	0.42(2)	0.681(2)							
Mg	2a	0	0	0	0.42(2)	0.319(2)							
O	4f	1/3	2/3	0.0907(5)	0.76(4)	1*							
(b) S.G.: $P6_3/mmc$		a	2.8881(2) \AA	c	11.207(2) \AA	Rwp	2	Rb	6.97	Rf	5.77	χ^2	5.21
Atom	Wyckoff positions	X	Y	Z	Biso(\AA^2)	Occup.							
Na_e	2d	1/3	2/3	3/4	3.8(5)	0.388(1)							
Na_f	2b	0	0	1/4	3.1(2)	0.242(1)							
Mn	2a	0	0	0	0.4(1)	0.747(2)							
Mg	2a	0	0	0	0.4(1)	0.253(2)							
O	4f	1/3	2/3	0.1037(5)	1.04(2)	1*							

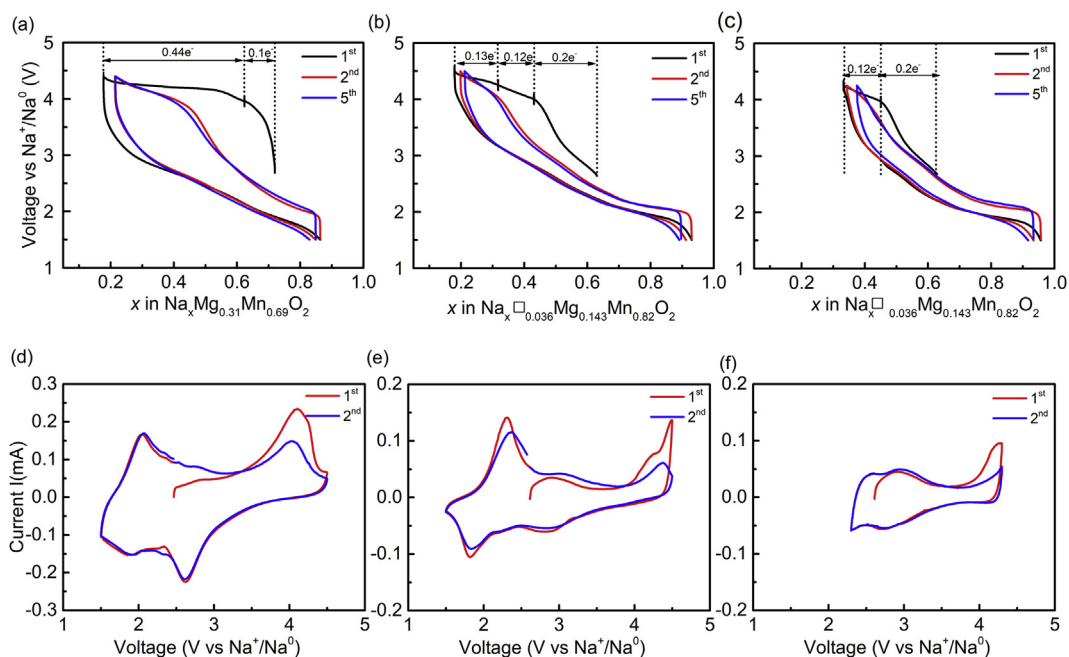


Fig. 3. (a) (b) (c) Voltage profile at C/20 at room temperature and (d) (e) (f) Cyclic voltammety profile at scan rate of 0.05 mV/s for of P2- $\text{Na}_{0.72}[\text{Mg}_{0.31}\text{Mn}_{0.69}]\text{O}_2$; $\text{Na}_{0.63}[\square_{0.036}\text{Mg}_{0.143}\text{Mn}_{0.82}]\text{O}_2$ in [1.5–4.5V] voltage range and $\text{Na}_{0.63}[\square_{0.036}\text{Mg}_{0.143}\text{Mn}_{0.82}]\text{O}_2$ in [1.5–4.15V] voltage range.

(0.14 and 0.24 for respectively $y = 0.3$ and $y = 0.15$) to Mn^{4+} . Above 4 V, the presence of voltage plateau domains indicates the existence of additional oxidation processes besides Mn oxidation. For $y = 0.3$ compound it corresponds to an extra capacity of 127 mAhg^{-1} (0.44 Na) associated to one plateau (4.2 V) while for $y = 0.15$, it corresponds to two voltage plateaus (4.1 V and 4.35 V) associated to capacity of respectively

$\sim 34 \text{ mAhg}^{-1}$ (0.12 Na) and $\sim 36 \text{ mAhg}^{-1}$ (0.13 Na).

Along the first discharge both compounds uptake more sodium (around 0.7 Na) than released on charge leading to a discharge capacity of $\sim 198 \text{ mAh g}^{-1}$ and the high voltage plateaus observed in the first charge are converted to a S shape voltage profile coupled with a large hysteresis. This peculiar profile is well known to be the electrochemical

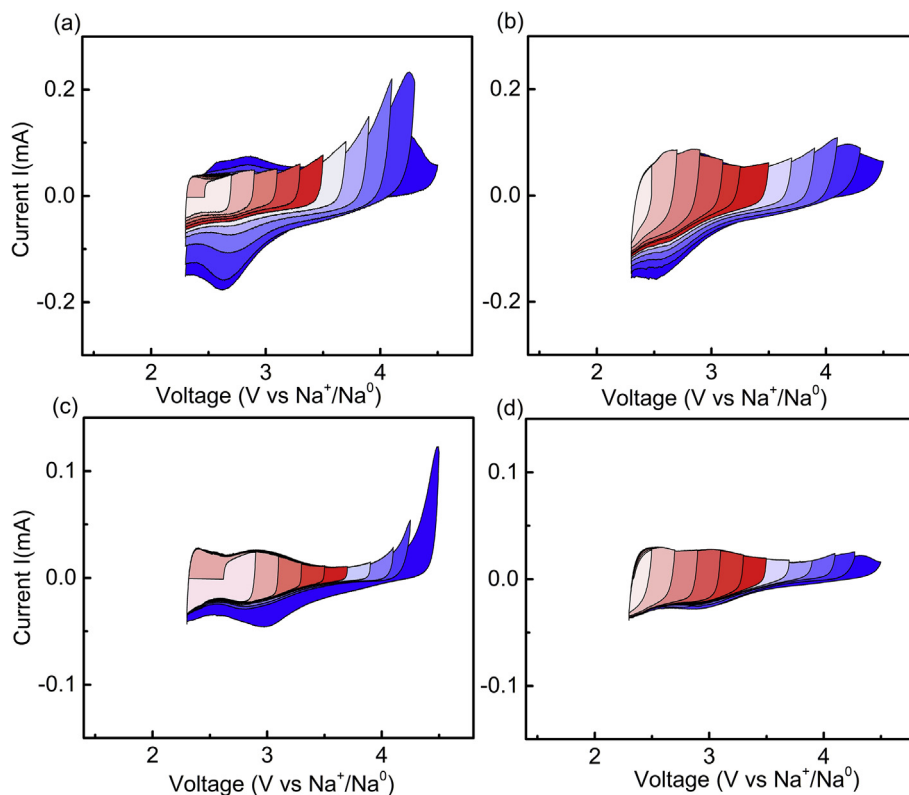


Fig. 4. Voltammety technique through gradual enlargement of upper voltage limit up to 4.5V on (a, c) a new cell and (b, d) on a cell after 3 cycles vs. Na^+/Na^0 in 3-electrode Swagelok type cell at scan rate of 0.05 mV/s for (a,b) sample P2- $\text{Na}_{0.72}[\text{Mg}_{0.31}\text{Mn}_{0.69}]\text{O}_2$ and (c,d) sample P2- $\text{Na}_{0.63}[\square_{0.036}\text{Mg}_{0.143}\text{Mn}_{0.82}]\text{O}_2$ respectively.

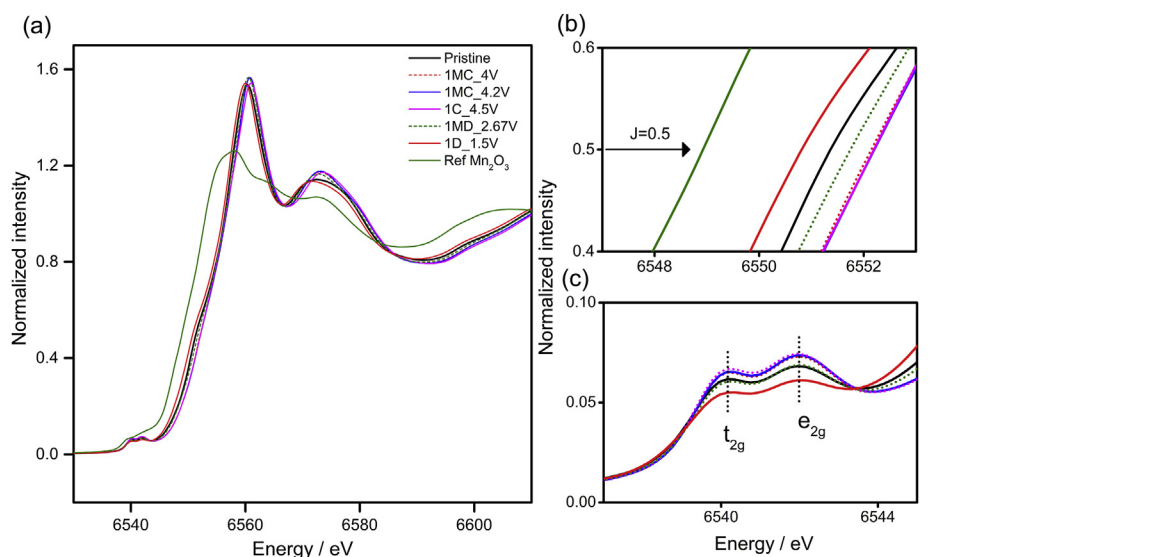


Fig. 5. (a) Mn K-edge XANES spectra of *ex-situ* $\text{Na}_{0.63}[\square_{0.036}\text{Mg}_{0.143}\text{Mn}_{0.82}]\text{O}_2$ including pristine, mid-charged (4V), mid-charged (4.2V), fully charged (4.5V), mid-discharged (2.67V) and fully discharged (1.5V) states, compared with some selected references for Mn^{3+} (Mn_2O_3). (b) zoom of the edge region, where Jump = 0.5 (c) zoom of the pre-edge region.

fingerprint of materials exhibiting oxygen redox activity.

The following charge profiles show a larger sloping domain from 1.5 V to around 4 V, followed by a single quasi flat plateau at around 4.2 V for both compounds corresponding to the removal of 0.23 Na ($\sim 67\text{mAhg}^{-1}$) and 0.12 Na ($\sim 34\text{mAhg}^{-1}$) for respectively $y = 0.3$ and $y = 0.15$ samples. This shows that the voltage plateau observed at 4.1 V along the first charge is not recovered along the second charge indicating that it should be associated to an irreversible process.

Along the next discharge process, the remaining plateaus convert to S shape voltage profile with large hysteresis characteristic of anionic redox process before reaching the typical sloping domain with low polarization characteristic of cationic redox processes. Even if in both samples the large hysteresis characteristic of anionic redox process is observed, the domain in capacity over which it is observed is shorter for $y = 0.15$ than for $y = 0.3$ as only Mg doping trigger anionic redox couple.

The following charge/discharge profiles perfectly superimpose showing the absence of drastic extra changes in the electrochemical processes.

To clearly identify the origin of the obvious change in the number of high voltage plateaus from first to second charge observed for $y = 0.15$ compound, a new experiment is performed with upper cut off voltage set to 4.3 V to prevent the access to the highest voltage plateau (4.35 V). The corresponding voltage profile reported in Fig. 3c shows that along the first charge the voltage plateau at around 4.1 V is observed with a capacity $\sim 34\text{mAhg}^{-1}$ (0.12 Na) equivalent to the first experiment. Along the first discharge, it is converted to sloping profile with a low hysteresis and is not recovered along the second charge which exhibits only a sloping profile. This new electrochemical profile is then stable over the following cycles with small voltage hysteresis observed over the whole investigated voltage range. The comparison of profiles obtained for $y = 0.15$ in the two different voltage ranges confirms that the voltage plateau occurring at 4.1 V is associated to an irreversible process.

To get a better visualization on the redox couples involved, cyclic voltammetry (CV) experiment is performed in a 3 electrode Swagelok cell at a low scan rate $v = 0.05\text{mV/s}$ in voltage range [1.5 4.5 V] for both samples and also in the narrowed [2.3 4.3 V] voltage range for the low Mg content sample. The electrochemical curves obtained in the [1.5 4.5 V] reported in Fig. 3d for $y = 0.3$ sample show the presence upon first positive polarization of two anodic peaks (2 V and 4.2 V) and two cathodic ones (1.8 V and 2.6 V). For the sample $y = 0.15$, the electrochemical curves (Fig. 3e) collected in the same [1.5 4.5 V] voltage range

shows a more complex behavior enlisting upon first positive polarization four anodic peaks (three sharp at 2.3 V, 4.1 V, 4.35 V; one broad at 2.8 V) and only two cathodic peaks (one sharp at 1.8 V; one broad at 2.6 V). Upon following polarizations, for $y = 0.3$ sample, only a large decrease in the intensity of the anodic peak current at 4.2 V is observed, while for $y = 0.15$ sample, one anodic peak fully disappeared, only three anodic peaks (at 2.3 V, 2.8 V, 4.2 V) remain, and the two cathodic peaks (at 1.8 V and 2.6 V) are still observed. Here again to confirm the irreversibility of one of the electrochemical processes, a new experiment in narrow [2.3 4.25 V] voltage range is performed for $y = 0.15$ sample. The electrochemical curve reported in Fig. 3f shows that beside the suppression of pair of peaks excluded by selected voltage windows, the anodic peak at 4.2 V observed upon first positive polarization is not associated to a cathodic peak which confirms that the corresponding redox process is fully irreversible.

To correctly couple the anionic and cathodic peaks, new cyclic voltammetry experiments were conducted starting with positive polarization and gradually opening the voltage window toward higher voltages. In a first experiment, the low voltage cut off is maintained to 1.5 V for $y = 0.3$ sample and allows confirming the allocation of the Mn redox couple (Figure SI 1). For all the other experiments the low voltage cut off is maintained at 2.3 V to focus only on high voltage phenomena. The results obtained while maintaining the low voltage cut off at 2.3 V presented in Fig. 4a and c for respectively $y = 0.3$ and $y = 0.15$ shows that the anodic peaks at high voltage (between 4.1 and 4.5 V) are compensated by only one cathodic peak at around 2.8 V. This shows that, for $y = 0.15$, the first anodic peak at 4.2 V is not significantly compensated upon negative polarization which confirms that the associated redox process is irreversible. To evidence if such an irreversibility is partial and occurs progressively along cycling, new cells were assembled and cycled 5 times before conducting the same cyclic voltammetry technique with progressive opening of the voltage window (Fig. 4b and d). The absence of obvious changes in the intensity of cathodic and anodic peaks confirms that the irreversible phenomenon occurs only at the first cycle.

To correctly couple the anionic and cathodic peaks, new cyclic voltammetry experiments were conducted starting with positive polarization and gradually opening the voltage window toward higher voltages. In a first experiment, the low voltage cut off is maintained to 1.5 V for $y = 0.3$ sample and allows confirming the allocation of the Mn redox couple (Figure SI 1). For all the other experiments the low voltage cut off is maintained at 2.3 V to focus only on high voltage phenomena. The results obtained while maintaining the low voltage cut off at 2.3 V presented in Fig. 4a and c for respectively $y = 0.3$ and $y = 0.15$ shows that the anodic peaks at high voltage (between 4.1 and 4.5 V) are compensated by only one cathodic peak at around 2.8 V. This shows that, for $y = 0.15$, the first anodic peak at 4.2 V is not significantly compensated upon negative polarization which confirms that the associated redox process is irreversible. To evidence if such an irreversibility is partial and occurs progressively along cycling, new cells were assembled and cycled 5 times before conducting the same cyclic voltammetry technique with progressive opening of the voltage window (Fig. 4b and d). The absence of obvious changes in the intensity of cathodic and anodic peaks confirms that the irreversible phenomenon occurs only at the first cycle.

To correctly couple the anionic and cathodic peaks, new cyclic voltammetry experiments were conducted starting with positive polarization and gradually opening the voltage window toward higher voltages. In a first experiment, the low voltage cut off is maintained to 1.5 V for $y = 0.3$ sample and allows confirming the allocation of the Mn redox couple (Figure SI 1). For all the other experiments the low voltage cut off is maintained at 2.3 V to focus only on high voltage phenomena. The results obtained while maintaining the low voltage cut off at 2.3 V presented in Fig. 4a and c for respectively $y = 0.3$ and $y = 0.15$ shows that the anodic peaks at high voltage (between 4.1 and 4.5 V) are compensated by only one cathodic peak at around 2.8 V. This shows that, for $y = 0.15$, the first anodic peak at 4.2 V is not significantly compensated upon negative polarization which confirms that the associated redox process is irreversible. To evidence if such an irreversibility is partial and occurs progressively along cycling, new cells were assembled and cycled 5 times before conducting the same cyclic voltammetry technique with progressive opening of the voltage window (Fig. 4b and d). The absence of obvious changes in the intensity of cathodic and anodic peaks confirms that the irreversible phenomenon occurs only at the first cycle.

3.3. Charge compensation mechanism

Based on similarities of electrochemical curves obtained for $y = 0.3$ and $y = 0.15$ samples with reported ones [8,10,12,17], we can associate unambiguously the high voltage phenomena observed in $\text{P2 Na}_{0.72}[\text{Mg}_{0.31}\text{Mn}_{0.69}]\text{O}_2$ to oxygen redox activity and suggest that

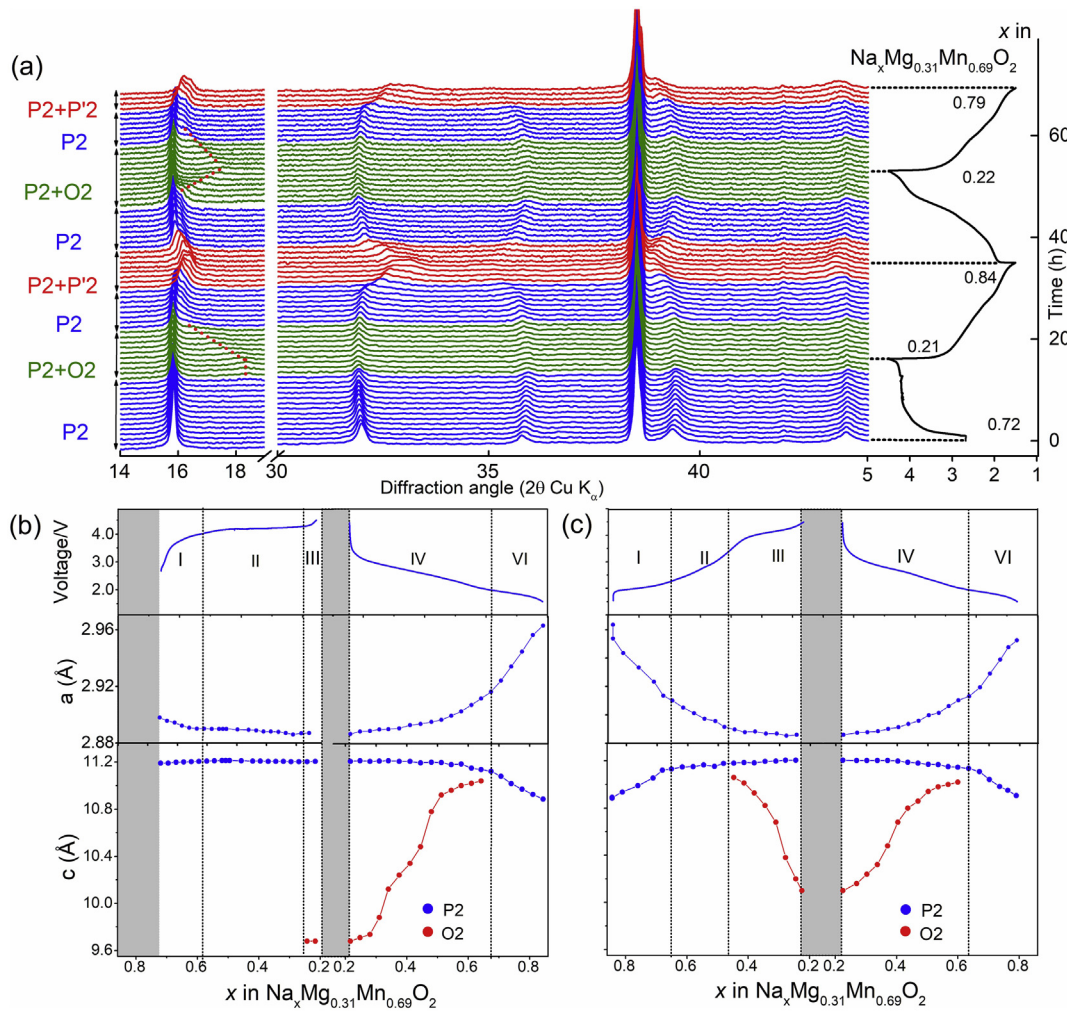


Fig. 6. (a) *operando* XRD pattern of P2 type $\text{Na}_{0.72}[\text{Mg}_{0.31}\text{Mn}_{0.69}]\text{O}_2$ upon 2 cycles as a function of Na amount at C/30 (The corresponding time versus voltage plot is shown on the right) and evolution of refined cell parameter a_{P2} and c_{P2} upon (b) first cycle and (c) second cycle.

both high voltage plateaus observed for P2 $\text{Na}_{0.63}[\square_{0.036}\text{Mg}_{0.143}\text{Mn}_{0.820}]\text{O}_2$ are also related to anionic redox phenomena. To avoid duplication of already reported results, main characterization of $y = 0.15$ sample is given in SI. The XAS experiments have been carried out to follow mainly the evolution of Mn valence state and therefore to infer the oxygen participation. The Mn K edge normalized XANES spectra for the *ex situ* samples ($y = 0.15$) at different states of charge are reported in Fig. 5. The Mn K edge shifts towards higher energy from pristine (6551.4 eV) to sample charged at 4 V (6552.2 eV) then remains unchanged for samples charged up to 4.2 V and 4.5 V. It indicates that the Mn reaches 4+ oxidation state at 4 V where the sloping domain observed in electrochemical curve is ended and keeps in 4+ state over the domain of two high voltage plateaus. Upon discharge, the Mn K edge shifts back towards lower energy from 6552.2 eV at full discharge to 6551.8 eV at mid discharge (2.67 V) and finally to 6550.8 eV at full discharge down to 1.5 V. Despite insertion of 0.3 Na at the beginning of the discharge, the small shift of Mn K edge clearly indicates that, in this domain, Mn is only slightly reduced and gives an indirect proof of the participation of O redox couple at early stage of sodiation. Upon further sodiation down to 1.5 V, the large shift (around 1 eV) of Mn K edge reveals that Mn is more reduced than in pristine compound, in agreement with the obtained composition $\text{Na}_1\text{Mg}_{0.14}\text{Mn}_{0.82}\text{O}_2$. The increase in intensity of the pre peak upon first charge indicates a change in the Mn environment attributed to distortions of the MnO_6 octahedra, as already reported in several compounds exhibiting anionic redox activity [20–22]. The further decrease in intensity of the pre peak during first discharge until 1.5 V indicates the MnO_6 distortion is dominated by the Jahn teller

effect, as large amount of Mn is reduced to 3+.

3.4. Structural evolution upon cycling

The evolution of the *operando* XRD patterns collected during galvanostatic experiments at C/30 in the [1.5V–4.5 V] voltage range as well as the refined cell parameters are reported in Fig. 6 and Fig. 7, for respectively $y = 0.3$ and $y = 0.15$ samples. For clarity, regions of identical behavior (solid solution or bi-phasic processes) are visualized (using roman numbers) for both charge and discharge processes. At the beginning of the charge (Region I), the behavior of both compounds is similar. The desodiation is accompanied by a solid solution process with a decrease in a_{P2} lattice parameter in agreement with the oxidation of remaining Mn^{3+} to smaller Mn^{4+} (contraction of MnO_6 octahedra) and an increase in c_{P2} lattice parameter due to increased repulsive O–O effect (smaller Na screening effect). Upon further desodiation where activation of anionic redox is triggered (Region II and III), only a broadening of the peaks associated to the growing of stacking faults [23] is observed while lattice parameters remain constant. Despite this is expected for the a_{P2} lattice parameter since Mn stays at +4 valence state, it is more surprising for the c_{P2} lattice parameter for which continuous Na removal should lead to a lowering of the screening effect and so to increase in the O–O repulsive effect. This apparent discrepancy will be discussed later. While for $y = 0.15$ sample this process occurs up to the fully charged state, for $y = 0.3$ compound the growing of an additional broad diffraction peak at 18.4° indicates the appearance of a new phase (Region III in Fig. 6b). The

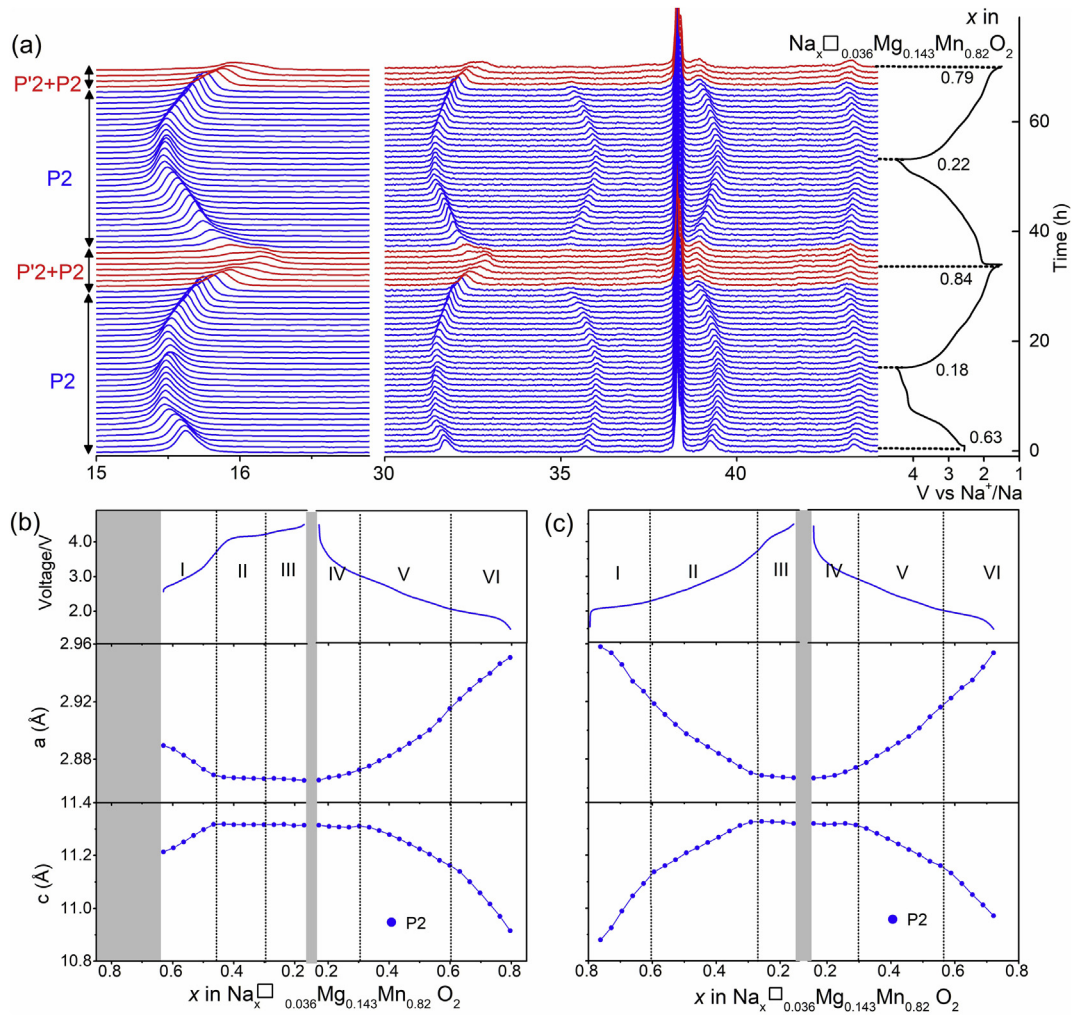


Fig. 7. (a) *operando* XRD patterns of P2 type $\text{Na}_{0.63}[\square_{0.036}\text{Mg}_{0.143}\text{Mn}_{0.82}]\text{O}_2$ upon 2 cycles as a function of Na amount at C/30 (The corresponding time versus voltage plot is shown on the right) and evolution of refined cell parameter a_{P2} and c_{P2} upon (b) first cycle and (c) second cycle.

calculated interlayer distance (4.82 Å) being close to the d value of O2 type structure [24] and much more shorter than the one of OP4 [13, 25] or Z [17,26] phase (5.1–5.2 Å), we can consider that O2 type is formed at the end of charge of the $y = 0.3$ sample. Upon the first discharge, the $y = 0.3$ and $y = 0.15$ samples undergo different structural evolutions. For $y = 0.15$, the c_{P2} lattice parameter (Fig. 7b) remains constant at the early beginning of the sodiation process (Region IV) and then gradually decreases until insertion of around 0.6Na following a solid solution process (Region V) in a perfect symmetric way compared to the first charge. For $y = 0.3$, the c_{P2} lattice parameter (Fig. 6b) remains constant over the full sodiation range up to 0.6 inserted Na (Region IV and V). However, a gradual and continuous shift of the (002)_{O2} peak towards lower angle is observed until it merges with the (002)_{P2} peak for 0.6 inserted Na. The structural evolution of $y = 0.3$ sample indicates that a bi-phasic mechanism is at the origin of the formation of O2 type phase at the end of the first charge but that the first sodiation follows a solid solution mechanism occurring only on the O2 type phase. In addition, the gradual shift of (002)_{O2} peak indicates that the increase in the screening effect is larger than the increase in the oxygen negative charge leading, when the large interlayer distance is reached, to the conversion from O2 type structure to more stable prismatic surrounding for Na *i.e.* to P2 type structure. Above 0.6 Na inserted (Region VI), both compounds consist of only P2 type phase and show similar evolution of cell parameters (Figs. 6b and 7b), in agreement with reduction of Mn^{4+} to Mn^{3+} and increasing of Na screening effect, confirming the existence of a solid solution process. In addition, the splitting of (00l) peaks and growing of a

small peak at 35° suggest the conversion from P2 to P'2 type structure in agreement with distortions induced by the cooperative Jahn Teller effect of Mn^{3+} [17]. Upon second charge (Figs. 6c and 7c), the P'2 to P2 transition occurs at early stage of desodiation (Region I) and then the evolution of P2 type lattice parameters characteristic of a solid solution process is observed in the region where Mn is electrochemically active (Region II). At the highest state of charge (Region III), no evolution of the P2 type lattice parameters is observed for both compounds. The growing and shifting of (002)_{O2} peaks observed for $y = 0.3$ sample, is perfectly symmetric as compared to the first discharge which confirms the reversibility of the structure transition. For both $y = 0.15$ and $y = 0.3$ samples, the second charge is then perfectly symmetric to the first discharge showing that irreversibility is observed only along the first cycle.

4. Discussion

The comparative analysis of the studied compounds ($y = 0.15$ and $y = 0.3$) shows that despite they belong to the solid solution P2 $\text{Na}_x\text{Mn}_{1-y}\text{Mg}_y\text{O}_2$, the low Mg content compound exhibits vacancies in the transition metal oxide layer while no vacancies have been evidenced in the high Mg content compound. The latter is close to the already widely studied P2 $\text{Na}_{2/3}\text{Mg}_{0.28}\text{Mn}_{0.72}\text{O}_2$ [8,18] showing, among others, the activation of anionic redox corresponding, in the voltage curve, to a plateau at around 4.2 V. Interestingly, the electrochemical behavior of P2 $\text{Na}_{0.63}[\square_{0.036}\text{Mg}_{0.143}\text{Mn}_{0.82}]\text{O}_2$ shows during the first charge two

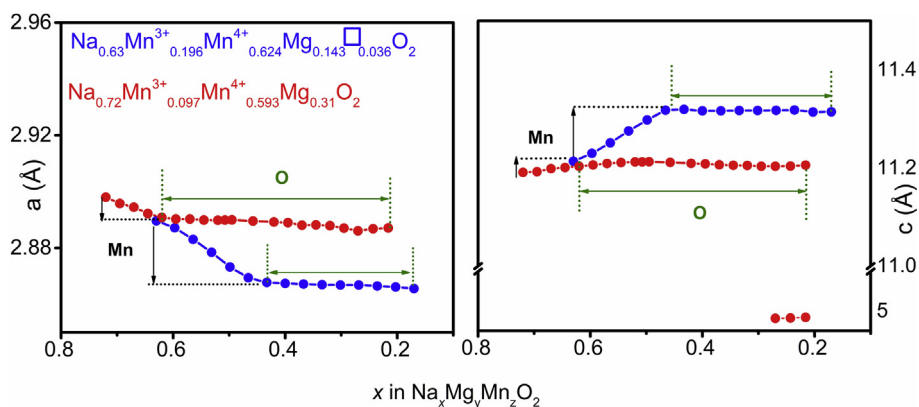


Fig. 8. Evolution of refined cell parameters a and c upon first charge with identification of redox domain for samples $\text{Na}_{0.63}[\square_{0.036}\text{Mg}_{0.143}\text{Mn}_{0.82}]\text{O}_2$ and $\text{Na}_{0.72}[\text{Mg}_{0.31}\text{Mn}_{0.69}]\text{O}_2$.

high voltage plateaus, both corresponding to the redox contribution of oxygen. This indicates that the presence of Mg or vacancies in the surrounding of oxygen gives rise to non bonding $|\text{O}_{2p}$ states at two different energies. This shows that randomly distributed Mg and vacancies have a distinct effect on the electronic structure. Moreover, in agreement with the proposed relationship showing that the lower the cationic charge around one oxygen is, the higher in energy its $|\text{O}_{2p}$ states is expected [27], the energy of the $|\text{O}_{2p}$ state along Na O \square (zero cationic charge) should be higher than the one along Na O Mg. This allows attributing the lowest (4.1 V)/highest (4.35 V) voltage plateaus to respectively vacancies/Mg doping activated anionic redox couples.

We can therefore also conclude that among both anionic redox processes, only the one triggered by vacancies is irreversible. This is in agreement with reported poor reversibility of vacancies activated anionic redox in similar compounds e.g. O3 $\text{Li}[\text{Ni}_{1/6}\square_{1/6}\text{Mn}_{2/3}]\text{O}_2$ [28] and P2 $\text{Na}_{0.754}[\square_{0.065}\text{Ni}_{0.241}\text{Mn}_{0.693}]\text{O}_2$ [11]. In these compounds

it has been speculated that the irreversibility is due to whether the elimination of the vacancies caused by local structural distortion or irreversible phase transition [29]. The absence of phase transition, as deduced by *operando* XRD, privileges the local structural distortion as the source of the irreversibility of the anionic redox process associated to vacancies. This contrasts with the reversibility of the anionic redox activity observed for $\text{Na}_{4/7-x}[\square_{1/7}\text{Mn}_{6/7}]\text{O}_2$ ($\text{Na}_2\text{Mn}_3\text{O}_7$) [19] in which the ordering of vacancies is speculated to create homogenous $\text{Na}^+ \square$ coulombic attraction which stabilizes the stacking of TM layers upon sodiation [9,10]. The relationship between ordering and reversibility is in accordance with the reversibility of Mg doping activated anionic redox observed for $y = 0.15$ and $y = 0.3$ samples both exhibiting, in pristine material, Mg ordering as evidenced by the presence of superstructure peaks in XRD patterns (Fig. 1). Then it can be concluded that while several sources (vacancies or adequate doping) can trigger anionic redox activity, their distribution in the pristine compound over the TM layer

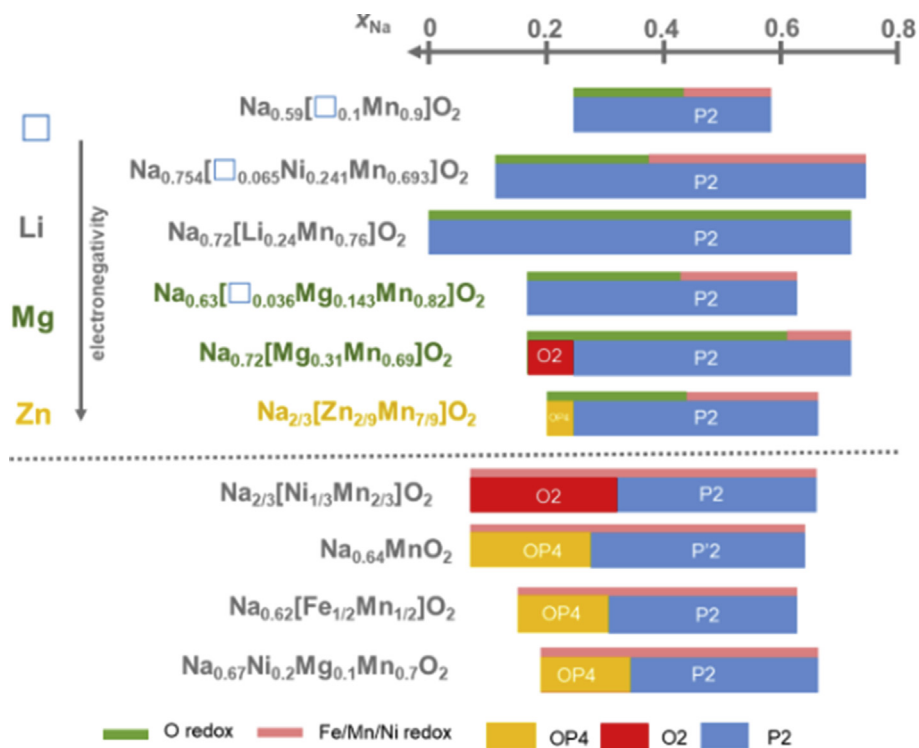


Fig. 9. Summary of phase evolution versus Na content upon first charge for $\text{Na}_{0.63}[\square_{0.036}\text{Mg}_{0.143}\text{Mn}_{0.82}]\text{O}_2$, $\text{Na}_{0.72}[\text{Mg}_{0.31}\text{Mn}_{0.69}]\text{O}_2$ with other reported anionic redox active compounds $\text{Na}_{2/3}\text{Zn}_{2/9}\text{Mn}_{7/9}\text{O}_2$ [12], $\text{Na}_{0.59}[\square_{0.1}\text{Mn}_{0.9}]\text{O}_2$ [13], $\text{Na}_{0.754}[\square_{0.065}\text{Ni}_{0.241}\text{Mn}_{0.693}]\text{O}_2$ [11], $\text{Na}_{0.72}\text{Li}_{0.24}\text{Mn}_{0.76}\text{O}_2$ [30], and non-anionic redox compounds $\text{Na}_{2/3}[\text{Ni}_{1/3}\text{Mn}_{2/3}]\text{O}_2$ [24], $\text{Na}_{0.67}\text{Ni}_{0.2}\text{Mg}_{0.1}\text{Mn}_{0.7}\text{O}_2$ [31], $\text{Na}_{0.62}[\text{Fe}_{1/2}\text{Mn}_{1/2}]\text{O}_2$ [17], P'2- $\text{Na}_{0.64}\text{MnO}_2$ [13].

seems to govern the reversibility of the process.

Beside the absence of clear irreversible structure changes, the *operando* XRD analysis allows evidencing that the activation of anionic redox couple leads to a change in the evolution of cell parameters. The comparison of the refined lattice parameters for both $y = 0.3$ and $y = 0.15$ samples (Fig. 8) shows that, beside the conventional evolution associated to Mn^{4+}/Mn^{3+} redox couple, both a_{P2} and c_{P2} lattice parameters remain constant on the whole composition range corresponding to the activation of anionic redox. As discussed previously, upon charge the decrease in a_{P2} reflects the oxidation from Mn^{3+} to Mn^{4+} and the increase in c_{P2} is ascribed to the increased repulsive O-O effect brought by the decrease of Na screening. In the domain where oxygen redox couple is active, Mn remains at the +4 valence state explaining the absence of variation of the a_{P2} lattice parameter. The absence of variation of c_{P2} indicates that the lowering of the negative charge associated to the oxidation of oxygen balances perfectly the lowering of screening effect due to continuous Na removal. Moreover, the P to O structure change typically correlated to the increase in the repulsive effect between oxygen of adjacent layers is not observed for $y = 0.15$ and appears only at highest state of charge for $y = 0.3$. Interestingly, the comparison of the P2 type stability domain upon first charge (Fig. 9) determined in this study with reported ones for compounds exhibiting combination of both anionic and cationic redox couples ($Na_{0.59}[□_{0.1}Mn_{0.9}]O_2$ [13], $Na_{0.754}[□_{0.065}Ni_{0.241}Mn_{0.693}]O_2$ [11], $Na_{0.72}Li_{0.24}Mn_{0.76}O_2$ [30]) and non anionic redox compounds ($Na_{2/3}[Ni_{1/3}Mn_{2/3}]O_2$ [24], $Na_{0.67}Ni_{0.2}Mg_{0.1}Mn_{0.7}O_2$ [31], $Na_{0.62}[Fe_{1/2}Mn_{1/2}]O_2$ [17], $P'2 Na_{0.64}MnO_2$ [13]) shows an equivalent trend. All compounds with anionic redox activity exhibit a stability domain of the P2 type structure largely expanded in the low Na content part compared to purely cationic redox active compounds. This confirms that the oxidation of oxygen balances the decrease in the screening effect and is beneficial for the stabilization of the P type structure. Besides the well established positive effect of anionic redox reaction in providing extra capacities for Na rich compounds, our results show that it also enables to stabilize the Na deficient P2 type structure at high state of charge. Surprisingly, such stabilizing effect seems not to be effective in O type structure. As evidenced in this study, O2 type structure once formed at highest states of charge, reacts with Na insertion/extraction following a solid solution process with increase/decrease in the interlayer space as evidenced by the gradually shift of $(002)_{O2}$ peaks. This may indicate that in this case the Na screening effect is not fully compensated by the corresponding change in the charge carried out by the oxygen.

5. Conclusion

We compared two members of the same solid solution in which we can discriminate the effects, on the anionic redox, of different activation sources (vacancies, Mg^{2+}) with the one associated to the cation vacancies occurring at lower voltage and being irreversible. We demonstrated the importance of the cation vacancies and Mg^{2+} distribution in ruling the reversibility of the anionic redox process with the process being irreversible when the vacancies are pinned to local structural distortion in a disorder way during the charging process and reversible when the Mg^{2+} distribution is ordered. Additionally, we provided evidence, via *operando* XRD, for enhancement of the compositional stability range of the P2 type structure till high state of charge which is consistent with the lowering of charge carried out by the oxygen due to the anionic redox process. Practically wise, this is beneficial as it enables to recover the capacity usually lost by the need to add electrochemically inactive element (such as Al, and many others) to stabilize P2 structure. Although anionic redox activity in layered oxides has been intensively studied, this work brings another dimension in decoupling the importance of cation vacancies vs highly electropositive cations (Mg^{2+}) in governing the activation and

reversibility of anionic redox process. Moreover, these results show that the activation of anionic redox is beneficial not only for Na rich but for all layered compounds even Na deficient ones, as it stabilizes the P2 type structure at high state of charge without capacity loss opposite to the use of electrochemically non active stabilizers.

Declaration of competing interest

The authors declare that they have no known competing financial interests or personal relationships that could have appeared to influence the work reported in this paper.

CRediT authorship contribution statement

Xue Bai: Investigation, Writing original draft. **Antonella Iadecola:** Investigation, Writing original draft. **Jean-Marie Tarascon:** Supervision, Writing review & editing. **Patrick Rozier:** Conceptualization, Writing original draft, Supervision.

Acknowledgements

X. B. thanks the French National network “Réseau sur le Stockage Electrochimique de l’Energie” (RS2E) FR CNRS 3459 and Agence Nationale de la Recherche (Label STORE EX) for financial support. J. M.T. acknowledge funding from the European Research Council (ERC) (FP/2014)/ERC Grant Project 670116 ARPEMA. This research has received funding from the European Union’s Horizon 2020 research and innovation programme under grant agreement 646433 Naiades. The authors also thank the synchrotron SOLEIL (France) for providing beamtime at the ROCK beamline financed by the French National Research Agency (ANR) as a part of the “Investissements d’Avenir” program (ANR 10 EQPX 45; proposal #20171234).

Appendix A. Supplementary data

Supplementary data to this article can be found online at <https://doi.org/10.1016/j.ensm.2020.05.032>.

References

- [1] M. Sathiya, G. Rousse, K. Ramesha, C.P. Laisa, H. Vezin, M.T. Sougrati, M.L. Doublet, D. Foix, D. Gonbeau, W. Walker, et al., Reversible anionic redox chemistry in high-capacity layered-oxide electrodes, *Nat. Mater.* 12 (9) (2013) 827–835, <https://doi.org/10.1038/nmat3699>.
- [2] A. Grimaud, W.T. Hong, Y. Shao-Horn, J.M. Tarascon, Anionic redox processes for electrochemical devices, *Nat. Mater.* 15 (2) (2016) 121–126, <https://doi.org/10.1038/nmat4551>.
- [3] N. Yabuuchi, Solid-state redox reaction of oxide ions for rechargeable batteries. <https://doi.org/10.1246/cl.161044>, 2016, 412–422.
- [4] B. Li, D. Xia, Anionic redox in rechargeable lithium batteries, *Adv. Mater.* 29 (48) (2017) 1–28, <https://doi.org/10.1002/adma.201701054>.
- [5] G. Assat, J.M. Tarascon, Fundamental understanding and practical challenges of anionic redox activity in Li-ion batteries, *Nat. Energy* 3 (5) (2018) 373–386, <https://doi.org/10.1038/s41560-018-0097-0>.
- [6] P. Rozier, M. Sathiya, A.R. Paulraj, D. Foix, T. Desaunay, P.L. Taberna, P. Simon, J.M. Tarascon, Anionic redox chemistry in Na-rich $Na_2Ru_1 - YSn_3O_3$ positive electrode material for Na-ion batteries, *Electrochem. Commun.* 53 (2015) 29–32, <https://doi.org/10.1016/j.elecom.2015.02.001>.
- [7] B. Mortemard De Boisse, G. Liu, J. Ma, S.I. Nishimura, S.C. Chung, H. Kiuchi, Y. Harada, J. Kikkawa, Y. Kobayashi, M. Okubo, et al., Intermediate honeycomb ordering to trigger oxygen redox chemistry in layered battery electrode, *Nat. Commun.* 7 (1) (2016) 1–9, <https://doi.org/10.1038/ncomms11397>.
- [8] U. Maitra, R.A. House, J.W. Somerville, N. Tapia-Ruiz, J.G. Lozano, N. Guerrini, R. Hao, K. Luo, L. Jin, M.A. Pérez-Osorio, et al., Oxygen redox chemistry without excess alkali-metal ions in $Na_2/3[Mg_{0.28}Mn_{0.72}]O_2$, *Nat. Chem.* 10 (3) (2018) 288–295, <https://doi.org/10.1038/nchem.2923>.
- [9] B. Mortemard de Boisse, S. ichi Nishimura, E. Watanabe, L. Lander, A. Tsuchimoto, J. Kikkawa, E. Kobayashi, D. Asakura, M. Okubo, A. Yamada, Highly reversible oxygen-redox chemistry at 4.1 V in $Na_4/7-x[□_{1/7}Mn_{6/7}]O_2$ (□: Mn vacancy), *Adv. Energy Mater.* 8 (20) (2018) 1800409, <https://doi.org/10.1002/aenm.201800409>.

- [10] Y. Li, X. Wang, Y. Gao, Q. Zhang, G. Tan, Q. Kong, S. Bak, G. Lu, X.Q. Yang, L. Gu, et al., Native vacancy enhanced oxygen redox reversibility and structural robustness, *Adv. Energy Mater.* 9 (4) (2019) 1803087, <https://doi.org/10.1002/aenm.201803087>.
- [11] C. Ma, J. Alvarado, J. Xu, R.J. Clément, M. Kodur, W. Tong, C.P. Grey, Y.S. Meng, Exploring oxygen activity in the high energy P2-type Na_{0.78}Ni_{0.23}Mn_{0.69}O₂ cathode material for Na-ion batteries, *J. Am. Chem. Soc.* 139 (13) (2017) 4835–4845, <https://doi.org/10.1021/jacs.7b00164>.
- [12] X. Bai, M. Sathiyaa, B. Mendoza-Sánchez, A. Iadecola, J. Vergnet, R. Dedryvère, M. Saubanère, A.M. Abakumov, P. Rozier, J.M. Tarascon, Anionic redox activity in a newly Zn-doped sodium layered oxide P2-Na₂/3Mn_{1-y}Zn_yO₂ (0 < y < 0.23), *Adv. Energy Mater.* 8 (32) (2018) 1802379, <https://doi.org/10.1002/aenm.201802379>.
- [13] S. Kumakura, Y. Tahara, K. Kubota, K. Chihara, S. Komaba, Sodium and manganese stoichiometry of P2-type Na₂/3MnO₂, *Angew. Chem. Int. Ed.* 55 (41) (2016) 12760–12763, <https://doi.org/10.1002/anie.201606415>.
- [14] J.W. Murray, L.S. Balistrieri, B. Paul, The oxidation state of manganese in marine sediments and ferromanganese nodules, *Geochem. Cosmochim. Acta* 48 (6) (1984) 1237–1247, [https://doi.org/10.1016/0016-7037\(84\)90058-9](https://doi.org/10.1016/0016-7037(84)90058-9).
- [15] N. Birkner, S. Nayeri, B. Pashaei, M.M. Najafpour, W.H. Casey, A. Navrotsky, Energetic basis of catalytic activity of layered nanophase calcium manganese oxides for water oxidation, *Proc. Natl. Acad. Sci. U. S. A.* 110 (22) (2013) 8801–8806, <https://doi.org/10.1073/pnas.1306623110>.
- [16] V. Briois, C. La Fontaine, S. Belin, L. Barthe, T. Moreno, V. Pinty, A. Carcy, R. Girardot, E. Fonda, ROCK: the new quick-EXAFS beamline at SOLEIL, in: *Journal of Physics: Conference Series*, 2016, <https://doi.org/10.1088/1742-6596/712/1/012149>.
- [17] B. Mortemard De Boisse, D. Carlier, M. Guignard, L. Bourgeois, C. Delmas, P2-NaxMn1/2Fe1/2O2 phase used as positive electrode in Na batteries: structural changes induced by the electrochemical (De)Intercalation process, *Inorg. Chem.* 53 (20) (2014) 11197–11205, <https://doi.org/10.1021/ic5017802>.
- [18] N. Yabuuchi, R. Hara, K. Kubota, J. Paulsen, S. Kumakura, S. Komaba, A new electrode material for rechargeable sodium batteries: P2-type Na₂/3[Mg_{0.28}Mn_{0.72}]O₂ with anomalously high reversible capacity, *J. Mater. Chem.* 2 (40) (2014) 16851–16855, <https://doi.org/10.1039/c4ta04351k>.
- [19] R. Stoyanova, D. Carlier, M. Sendova-Vassileva, M. Yoncheva, E. Zhecheva, D. Nihtianova, C. Delmas, Stabilization of over-stoichiometric Mn⁴⁺ in layered Na₂/3MnO₂, *J. Solid State Chem.* 183 (6) (2010) 1372–1379, <https://doi.org/10.1016/j.jssc.2010.04.024>.
- [20] H. Koga, L. Croguennec, M. Ménétrier, P. Mannezzies, F. Weill, C. Delmas, S. Belin, Operando X-ray absorption study of the redox processes involved upon cycling of the Li-rich layered oxide Li_{1.20}Mn_{0.54}Co_{0.13}Ni_{0.13}O₂ in Li ion batteries, *J. Phys. Chem. C* 118 (11) (2014) 5700–5709, <https://doi.org/10.1021/jp412197z>.
- [21] D. Buchholz, J. Li, S. Passerini, G. Aquilanti, D. Wang, M. Giorgetti, X-ray absorption spectroscopy investigation of lithium-rich, cobalt-poor layered-oxide cathode material with high capacity, *ChemElectroChem* 2 (1) (2015) 85–97, <https://doi.org/10.1002/celec.201402324>.
- [22] L. Simonin, J.F. Colin, V. Ranieri, E. Canévet, J.F. Martin, C. Bourbon, C. Baetz, P. Strobel, L. Daniel, S. Patoux, In situ investigations of a Li-rich Mn-Ni layered oxide for Li-ion batteries, *J. Mater. Chem.* 22 (22) (2012) 11316–11322, <https://doi.org/10.1039/c2jm31205k>.
- [23] N. Yabuuchi, R. Hara, M. Kajiyama, K. Kubota, T. Ishigaki, A. Hoshikawa, S. Komaba, New O₂/P₂-type Li-excess layered manganese oxides as promising multi-functional electrode materials for rechargeable Li/Na batteries, *Adv. Energy Mater.* 4 (13) (2014), <https://doi.org/10.1002/aenm.201301453>.
- [24] Z. Lu, J.R. Dahn, In situ X-ray diffraction study of P2-Na₂/3[Ni₁/3Mn₂/3]O₂, *J. Electrochem. Soc.* 148 (11) (2001) A1225, <https://doi.org/10.1149/1.1407247>.
- [25] N. Yabuuchi, M. Kajiyama, J. Iwatate, H. Nishikawa, S. Hitomi, R. Okuyama, R. Usui, Y. Yamada, S. Komaba, P2-Type Nax[Fe₁/2Mn₁/2]O₂ made from earth-abundant elements for rechargeable Na batteries, *Nat. Mater.* 11 (6) (2012) 512–517, <https://doi.org/10.1038/nmat3309>.
- [26] B. Mortemard De Boisse, D. Carlier, M. Guignard, E. Guerin, M. Duttine, A. Wattiaux, C. Delmas, Influence of Mn/Fe ratio on electrochemical and structural properties of P2-NaxMn1-yFeyO2 phases as positive electrode material for Na-ion batteries, *Chem. Mater.* 30 (21) (2018) 7672–7681, <https://doi.org/10.1021/acs.chemmater.8b02953>.
- [27] M. Ben Yahia, J. Vergnet, M. Saubanère, M.L. Doublet, Unified picture of anionic redox in Li/Na-ion batteries, *Nat. Mater.* 18 (2019) 496–502.
- [28] E. McCalla, A.W. Rowe, J. Camardese, J.R. Dahn, The role of metal site vacancies in promoting Li-Mn-Ni-O layered solid solutions, *Chem. Mater.* 25 (13) (2013) 2716–2721, <https://doi.org/10.1021/cm401461m>.
- [29] B.P. Hahn, J.W. Long, D.R. Rolison, Something from nothing: enhancing electrochemical charge storage with cation vacancies, *Acc. Chem. Res.* 46 (5) (2013) 1181–1191, <https://doi.org/10.1021/ar200238w>.
- [30] X. Rong, E. Hu, Y. Lu, F. Meng, C. Zhao, X. Wang, Q. Zhang, X. Yu, L. Gu, Y.S. Hu, et al., Anionic redox reaction-induced high-capacity and low-strain cathode with suppressed phase transition, *Joule* 3 (2) (2019) 503–517, <https://doi.org/10.1016/j.joule.2018.10.022>.
- [31] G. Singh, N. Tapia-Ruiz, J.M. López Del Amo, U. Maitra, J.W. Somerville, R. Armstrong, J.M. Martínez de Ilarduya, T. Rojo, P.G. Bruce, High voltage Mg-doped Na_{0.67}Ni_{0.3-x}Mg_xMn_{0.7}O₂ (x = 0.05, 0.1) Na-ion cathodes with enhanced stability and rate capability, *Chem. Mater.* (2016), <https://doi.org/10.1021/acs.chemmater.6b01935>.

Decoupling the effect of vacancies and electropositive cations on the anionic redox processes in Na based P2-type layered oxides.

Xue Bai, Antonella Iadecola, Jean-Marie Tarascon, Patrick Rozier

Chemical composition analysis

ICP-AES was carried out on selected $y=0.15$ and $y=0.3$ samples of the P2- $\text{Na}_x\text{Mg}_y\text{Mn}_{1-y}\text{O}_2$ solid solution. The results are summarized in Table SI-1. The measured weight fractions are converted to atomic composition using the normalization $\text{Mg}+\text{Mn}=1$.

(a)				(b)			
Sample	Element in wt%			Sample	Element in wt%		
	Na	Mg	Mn		Na	Mg	Mn
	18.0(3)	8.22(5)	41.1(3)		15.8(2)	3.81(8)	49.7(9)
Pristine	Elements in molar%			Pristine	Elements in molar%		
	0.78(1)	0.338(2)	0.748(5)		0.69(1)	0.157(3)	0.90(2)
	Normalize to molar%(Mg +Mn)=1				Normalize to molar%(Mg +Mn)=1		
	0.72(1)	0.311(2)	0.689(5)		0.65(1)	0.149(3)	0.85(2)

Table SI-1: Chemical composition analysis by ICP-AES for $\text{Na}_x\text{Mg}_y\text{Mn}_{1-y}\text{O}_2$ with (a) $y=0.3$ and (b) $y=0.15$.

Cyclic voltammetry:

To correctly couple the anionic and cathodic peaks observed in cyclic voltammetry experiments, new experiments are conducted starting with positive polarization and gradually opening the voltage window toward higher voltages. The result of such an experiment carried out on $\text{P2-Na}_{0.72}[\text{Mg}_{0.31}\text{Mn}_{0.69}]\text{O}_2$ is presented in the Figure SI-1 where each color shade area represents 100% coulombic efficiency of oxidative and anodic capacity. The gradual expansion, from low cut off voltage 1.5 V, of the voltage window for $y=0.3$ shows that the anodic peak at 2 V is compensated by the cathodic peak at 1.8 V (see orange color region in Figure SI-1) in agreement with reported voltage for Mn redox couple. The anodic peak current at 4.2 V is compensated by the cathodic peak at 2.6 V (see blue color region in Figure SI-1) and the current intensity of anodic peak after scanning beyond 4.1 V decreased drastically, which indicates the presence of certain degree of irreversibility.

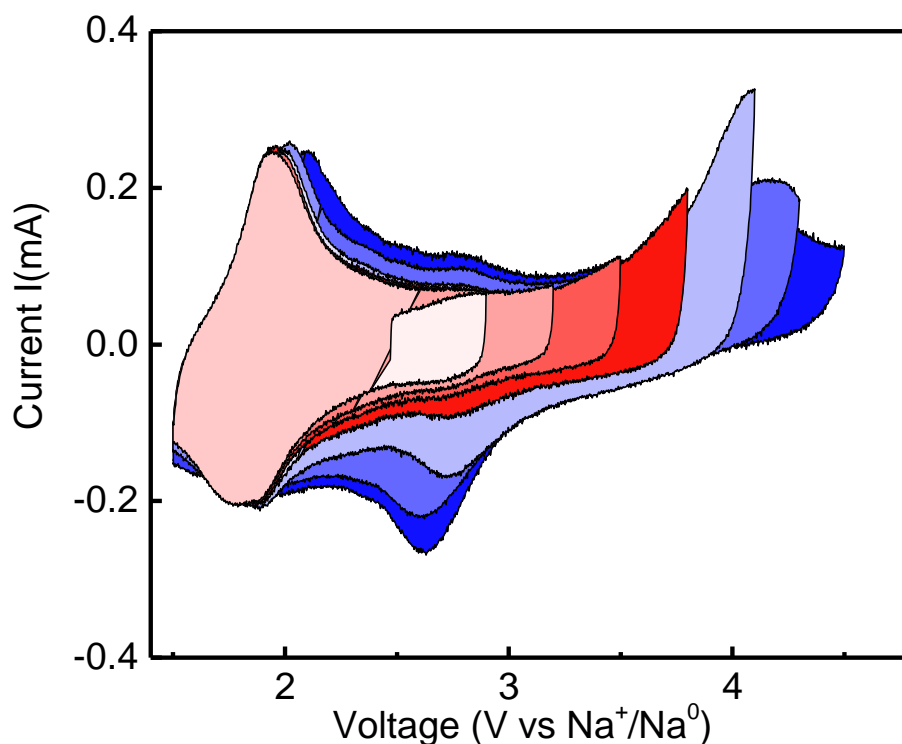


Figure SI-1: Cyclic voltammetry technique with gradual enlargement of upper voltage limit during the first cycle in the [1.5 or 2.3-4.5 V] vs. Na⁺/Na⁰ voltage for P2-Na_{0.72}[Mg_{0.31}Mn_{0.69}]O₂. Data are collected in 3-electrodes Swagelok type cell at scan rate of 0.05mV/s.

XAS experiments on *exsitu* P2-Na_{0.72}[Mg_{0.31}Mn_{0.69}]O₂

Ex situ XAS measurements at the Mn K-edge were performed in transmission mode at the ROCK beamline of synchrotron SOLEIL (France)¹⁶. A Si (111) channel-cut quick-XAS monochromator with an energy resolution of 0.8 eV at 8 keV and an oscillating frequency of 2 Hz was used. The intensity of the monochromatic X-ray beam was measured by three consecutive ionization detectors. A Mn foil was placed between the second and the third ionization chamber as reference. *Ex situ* samples at different states of charge/discharge were prepared as self-standing films which were pre-cycled at C/30 in hal cell vs Na, recovered from Swagelok cell, rinsed with DMC, dried in vacuum chamber and finally sealed in Kapton tape and plastic bag in glove box. *Ex situ* XAS spectra were treated using the Athena for energy calibration and normalization.

The results reported in the Figure SI-2 shows that Mn oxidation state in the pristine material is slightly lower than +4 in agreement with the stoichiometry. We consider the energy value obtained at half normalized energy step to follow the evolution of the oxidation state of Mn

Upon cycling, the Mn K-edge position is shifted toward higher energy corresponding to purely Mn^{4+} for mid-charged sample and remains unchanged for samples at fully charged state (4.5 V), mid-discharged states (3.2 V) and 2.5 V, excluding any Mn redox activity in this voltage range. Below 2.5 V, a large shift of around 1.5 eV toward lowest energy shows that the Mn is reduced and its oxidation state is close to +3 for the fully discharged sample (1.5 V). The increasing of pre-peak intensity upon first charge indicates a change in the local geometry of the MnO_6 octahedron, as already reported in several compounds exhibiting anionic redox activity^{2,3,4}. The further decreased intensity during first discharge until 1.5 V confirms the presence of MnO_6 distortion induced by the Jahn-teller effect, as large amount of Mn is reduced to 3+.

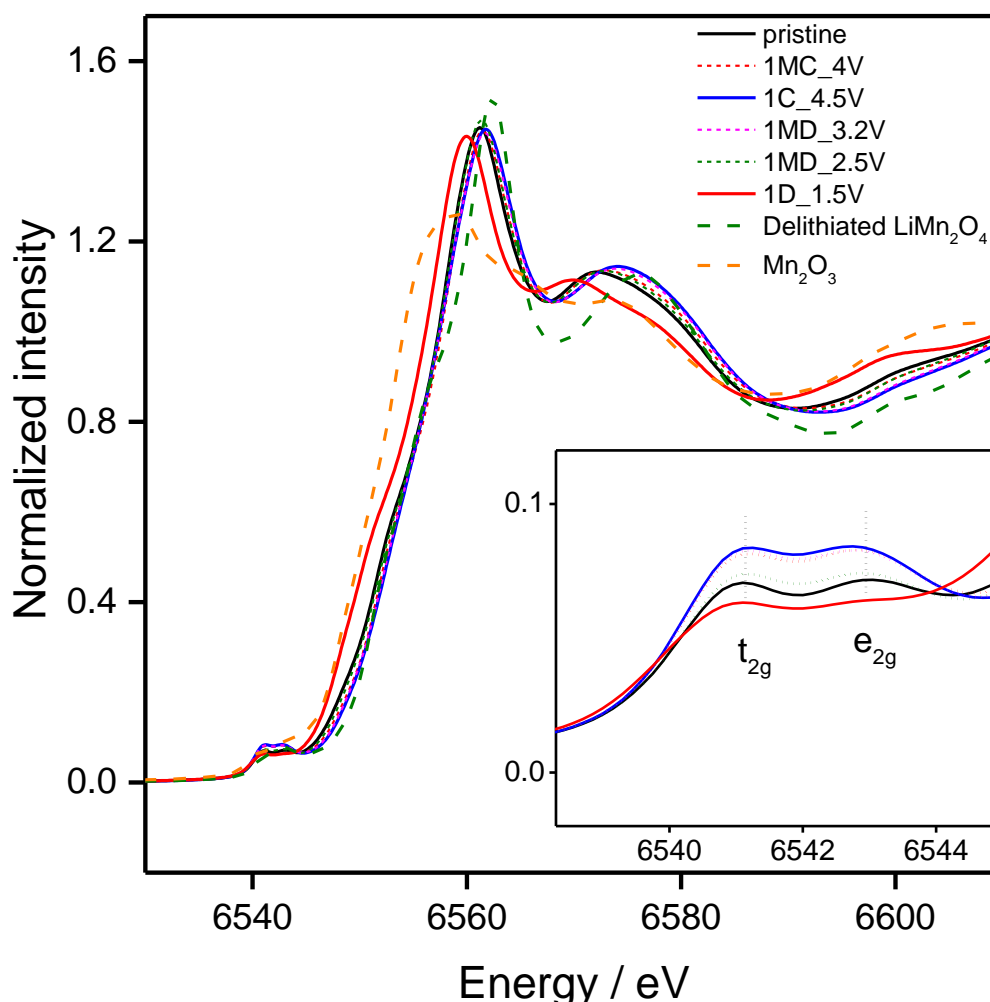


Figure SI-2: Mn K-edge XANES spectra of (a) *ex-situ* P2- $\text{Na}_{0.72}[\text{Mg}_{0.31}\text{Mn}_{0.69}]\text{O}_2$ including pristine, mid-charged(4 V), fully charged(4.5 V), mid-discharged(3.2 V), mid-discharge (2.5 V) and fully discharged (1.5 V) states, compared with some selected references for Mn^{3+} (Mn_2O_3) and Mn^{4+} (LiMn_2O_4 delithiated). The inset shows a zoom of the pre-edge region.

References

- (1) Briois, V.; La Fontaine, C.; Belin, S.; Barthe, L.; Moreno, T.; Pinty, V.; Carcy, A.; Girardot, R.; Fonda, E. ROCK: The New Quick-EXAFS Beamline at SOLEIL. In *Journal of Physics: Conference Series*; 2016. <https://doi.org/10.1088/1742-6596/712/1/012149>.
- (2) Koga, H.; Croguennec, L.; Ménétrier, M.; Mannesiez, P.; Weill, F.; Delmas, C.; Belin, S. Operando X-Ray Absorption Study of the Redox Processes Involved upon Cycling of the Li-Rich Layered Oxide $\text{Li}_{1.20}\text{Mn}_{0.54}\text{Co}_{0.13}\text{Ni}_{0.13}\text{O}_2$ in Li Ion Batteries. *J. Phys. Chem. C* **2014**, *118* (11), 5700–5709. <https://doi.org/10.1021/jp412197z>.
- (3) Buchholz, D.; Li, J.; Passerini, S.; Aquilanti, G.; Wang, D.; Giorgetti, M. X-Ray Absorption Spectroscopy Investigation of Lithium-Rich, Cobalt-Poor Layered-Oxide Cathode Material with High Capacity. *ChemElectroChem* **2015**, *2* (1), 85–97. <https://doi.org/10.1002/celec.201402324>.
- (4) Simonin, L.; Colin, J. F.; Ranieri, V.; Canévet, E.; Martin, J. F.; Bourbon, C.; Baehtz, C.; Strobel, P.; Daniel, L.; Patoux, S. In Situ Investigations of a Li-Rich Mn-Ni Layered Oxide for Li-Ion Batteries. *J. Mater. Chem.* **2012**, *22* (22), 11316–11322. <https://doi.org/10.1039/c2jm31205k>.